J. Fluid Mech. (2013), *vol.* 731, R4, doi:10.1017/jfm.2013.391

JFM RAPIDS
journals.cambridge.org/rapids

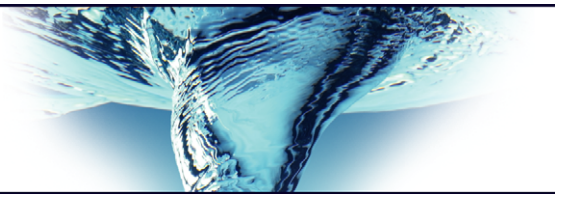

Coherent Lagrangian vortices: the black holes of turbulence

G. Haller[1] **and F. J. Beron-Vera**[2,†]

[1]Institute for Mechanical Systems, ETH Zurich, 8092 Zurich, Switzerland

[2]Rosenstiel School of Marine and Atmospheric Science, University of Miami, Miami, FL 33149, USA

(Received 13 May 2013; revised 18 July 2013; accepted 25 July 2013)

We introduce a simple variational principle for coherent material vortices in two-dimensional turbulence. Vortex boundaries are sought as closed stationary curves of the averaged Lagrangian strain. Solutions to this problem turn out to be mathematically equivalent to photon spheres around black holes in cosmology. The fluidic photon spheres satisfy explicit differential equations whose outermost limit cycles are optimal Lagrangian vortex boundaries. As an application, we uncover super-coherent material eddies in the South Atlantic, which yield specific Lagrangian transport estimates for Agulhas rings.

Key words: geophysical and geological flows, nonlinear dynamical systems, vortex flows

1. Introduction

Vortices in turbulence are often envisaged as rotating bodies of fluid, travelling as coherent islands in an otherwise incoherent ambient flow (Provenzale 1999). This Lagrangian view is appealingly simple, yet challenging to apply in actual vortex detection. The main difficulty is to classify fluid particle paths systematically as coherent or incoherent.

As a result, coherent features of turbulence are mostly described through instantaneous Eulerian quantities, such as velocity, pressure and their derivatives (cf. Jeong & Hussain 1985; Haller 2005, for reviews). In this approach, vortices are typically defined as regions of closed contours of an Eulerian scalar field, often with some added thresholding requirement. Such criteria can be highly effective in framing short-term features of the flow, even if the extracted coherent structures tend to be frame-dependent.

† Email address for correspondence: georgehaller@ethz.ch

Harry clarke's illustration for
'A Descent into the Maelström'
by Edgar Allan Poe (1841)

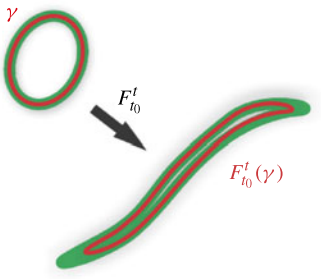

Typical material belt

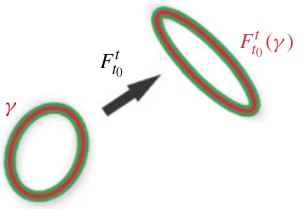

Coherent material belt

FIGURE 1. Edgar Allan Poe's maelstrom and material belts in turbulence. A closed material curve γ (red) at time t_0 is advected by the flow into its later position $F^t_{t_0}(\gamma)$ at time t. The advected curve remains coherent if an initially uniform material belt (green) around it shows no leading-order variations in stretching after advection.

In unsteady flow, however, Eulerian vortex boundaries are not material barriers. A fluid mass initialized in an Eulerian vortex will generally lose coherence, showing stretching and filamentation along the vortex path. The end-result for the fluid mass is widespread dispersion with little or no directionality (Beron-Vera *et al.* 2013). Yet the identification of coherent material vortices is becoming increasingly important in a number of areas. For instance, mesoscale oceanic eddies are broadly thought to carry water without substantial leakage or deformation. If their boundaries indeed resist filamentation, such eddies can create moving oases for the marine food chain (Denman & Gargett 1983), or even impact climate change through their long-range transport of salinity and temperature (Beal *et al.* 2011).

Lagrangian diagnostic tools show that some Eulerian vortices can carry fluid, but their leakage tends to be substantial (Provenzale 1999; Froyland *et al.* 2012). A rigorous approach to finding non-leaking material boundaries has recently emerged, but focuses only on relatively rare boundaries that maximize Lagrangian shear (Beron-Vera *et al.* 2013).

Parallel to these developments, coherent vortices are sometimes described as whirlpools, or maelstroms, in popular fiction. An early example can be found in Edgar Allan Poe's short story entitled *A Descent into a Maelström*:

> 'The edge of the whirl was represented by a broad belt of gleaming spray; but no particle of this slipped into the mouth of the terrific funnel ...'

This literary account depicts a belt-like vortex boundary that keeps particles from entering its interior (figure 1). Altogether, Poe's view on vortices is Lagrangian, and resonates with our intuition for black holes in cosmology.

As we show below, this view turns out to have some merit. When appropriately modelled, Poe's coherent belt becomes mathematically equivalent to a photon sphere, i.e. a surface on which light encircles a black hole without entering it. This analogy yields computational advantages, which we exploit in locating material eddy boundaries in the South Atlantic Ocean. Using satellite altimetry-based velocities from this region, we uncover super-coherent Lagrangian vortices, and derive estimates for coherent material transport induced by the Agulhas leakage.

2. Coherent material belts

We start with a two-dimensional velocity field of the form $v(x,t)$, with x labelling the location within an open region U of interest and with t referring to time. Fluid trajectories generated by $v(x,t)$ obey the differential equation

$$\dot{x} = v(x,t), \tag{2.1}$$

whose solutions are denoted $x(t;t_0,x_0)$, with x_0 referring to the initial position of the trajectory at time t_0. The evolution of fluid elements is described by the flow map

$$F_{t_0}^t(x_0) := x(t;t_0,x_0), \tag{2.2}$$

which takes any initial position x_0 to a later position at time t. Lagrangian strain in the flow is often characterized by the right Cauchy–Green strain tensor field $C_{t_0}^t(x_0) = \nabla F_{t_0}^t(x_0)^\top \nabla F_{t_0}^t(x_0)$, whose eigenvalues $\lambda_i(x_0)$ and eigenvectors $\xi_i(x_0)$ satisfy

$$C_{t_0}^t \xi_i = \lambda_i \xi_i, \quad |\xi_i| = 1, \quad i = 1,2; \quad 0 < \lambda_1 \leqslant \lambda_2, \quad \xi_1 \perp \xi_2. \tag{2.3}$$

Assume that $\varepsilon > 0$ is a minimal threshold above which we can physically observe differences in material strain over the time interval $[t_0,t]$. By smooth dependence on initial fluid positions (Arnold 1973), we will observe an $O(\varepsilon)$ variability in strain within an $O(\varepsilon)$ belt around a generic closed material curve γ. However, we seek exceptional γ curves around which $O(\varepsilon)$-thick coherent belts show no observable variability in their average straining (figure 1).

Such coherence in the strain field precludes nearby fluid elements from breaking away from γ. Again, by smooth dependence of finite-time strain on distance, the actual strain variability in such coherent, $O(\varepsilon)$-thick belts cannot be more than $O(\varepsilon^2)$.

To express this coherence principle mathematically, we select a parametrization $r(s)$ with $s \in [0,\sigma]$ for the closed curve γ at time t_0, and denote the length of a tangent vector $r'(s)$ by $l_{t_0}(s)$. We also let $l_t(s)$ denote the length of the corresponding tangent vector $(\mathrm{d}/\mathrm{d}s)F_{t_0}^t(r(s))$ along the advected curve $F_{t_0}^t(\gamma)$. These two tangent lengths can be calculated as

$$l_{t_0}(s) = \sqrt{\langle r'(s), r'(s)\rangle}, \quad l_t(s) = \sqrt{\langle r'(s), C_{t_0}^t(r(s))r'(s)\rangle}, \tag{2.4}$$

where $\langle\cdot,\cdot\rangle$ denotes the Euclidean inner product (Truesdell & Noll 2004). The averaged tangential strain along γ is then given by

$$Q(\gamma) = \frac{1}{\sigma}\int_0^\sigma \frac{l_t(s)}{l_{t_0}(s)}\,\mathrm{d}s. \tag{2.5}$$

As argued above, if an observable coherent material belt exists around γ, then on ε-close material loops we must have $Q(\gamma+\varepsilon h) = Q(\gamma) + O(\varepsilon^2)$, where $\varepsilon h(s)$ denotes small, periodic perturbations to γ. This is only possible if the first variation of Q vanishes on γ:

$$\delta Q(\gamma) = 0. \tag{2.6}$$

The calculus of variations applied to (2.6) leads to complicated differential equations that do not immediately provide insight (supplementary Appendix A; supplementary materials are available at http://dx.doi.org/10.1017/jfm.2013.391). However, as we show in supplementary Appendix B, any γ satisfying (2.6) also satisfies

$$\delta\mathscr{E}_\lambda(\gamma) = 0, \quad \mathscr{E}_\lambda(\gamma) = \int_0^\sigma \langle r'(s), E_\lambda(r(s))r'(s)\rangle\,\mathrm{d}s, \tag{2.7}$$

representing a closed stationary curve for the strain energy functional $\mathscr{E}_\lambda(\gamma)$ for some choice of the parameter $\lambda > 0$. Here, the tensor family

$$E_\lambda(x_0) = \tfrac{1}{2}\left[C^t_{t_0}(x_0) - \lambda^2 I\right] \tag{2.8}$$

denotes a generalization of the classic Green–Lagrange strain tensor $E_1(x_0) = [C^t_{t_0}(x_0) - I]/2$ (Truesdell & Noll 2004).

3. Lagrangian vortex boundaries

All stationary curves of $\mathscr{E}_\lambda$ that coincide with those of Q are found to have zero energy density (supplementary Appendix B), satisfying the implicit differential equation

$$\langle r'(s), E_\lambda(r(s))r'(s)\rangle = l^2_t(s) - \lambda^2 l^2_{t_0}(s) \equiv 0. \tag{3.1}$$

These material curves $r(s)$ are therefore uniformly stretched by the same factor λ when advected by the flow from time t_0 to time t. Such λ-lines serve as perfectly coherent cores for observably coherent material belts around them.

Equation (3.1) only admits non-degenerate $r(s)$ solutions on the flow domain U_λ where the two-dimensional tensor E_λ has non-zero eigenvalues of opposite sign. In this domain, the curves $r(s)$ are obtained as closed trajectories of one of the two explicit differential equations (supplementary Appendix C)

$$r'(s) = \eta^\pm_\lambda(r(s)), \quad \eta^\pm_\lambda = \sqrt{\frac{\lambda_2 - \lambda^2}{\lambda_2 - \lambda_1}}\,\xi_1 \pm \sqrt{\frac{\lambda^2 - \lambda_1}{\lambda_2 - \lambda_1}}\,\xi_2. \tag{3.2}$$

Such closed trajectories will occur in families of limit cycles parametrized by the stretching parameter λ. One can show that no two members of any such family can intersect (supplementary Appendix E). Thus a limit cycle of the vector field $\eta^\pm_\lambda$ will either grow or shrink under changes in λ, forming smooth annular regions of non-intersecting loops. The outermost member of such a band of coherent material loops will be observed physically as the Lagrangian vortex boundary. Indeed, immediately outside this boundary, no coherent material belts may exist in the flow.

4. Lagrangian vortices and black holes

The trajectories of (3.2), as stationary curves of the stretch energy $\mathscr{E}_\lambda(\gamma)$, admit an appealing geometric interpretation. First, note that on the domain U_λ, the quadratic function

$$g_\lambda(u, u) = \langle u, E_\lambda u\rangle \tag{4.1}$$

defines a Lorentzian metric, with signature $(-, +)$ inherited from the eigenvalue configuration of E_λ (Beem, Ehrlich & Kevin 1996). A Lorentzian metric extends the classic notion of distance to hyperbolic spaces. As such, it can also return zero or a negative value for the distance between two points that have a positive Euclidean distance.

Thus, (U_λ, g_λ) can be viewed as a two-dimensional Lorentzian manifold (Beem *et al.* 1996), or in the language of general relativity, a two-dimensional space–time. In such a space–time, light travels along null-geodesics of the Lorentzian metric, which are curves on which the Lorentzian metric vanishes identically. In our fluidic

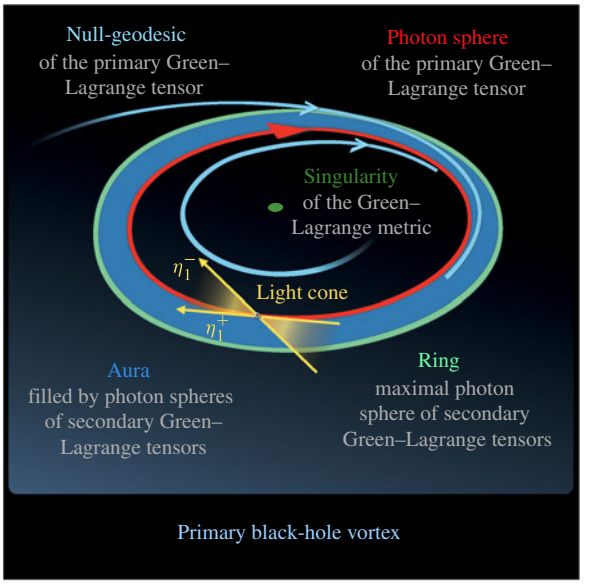

FIGURE 2. Mathematical equivalence between coherent Lagrangian vortices and black holes.

space–time (U_λ, g_λ), null-geodesics satisfy $g_\lambda(r'(s), r'(s)) \equiv 0$, and hence coincide with the λ-lines described in (3.1).

The closed λ-lines we have been seeking are therefore closed null-geodesics of g_λ. In cosmology, such null-geodesics occur around black holes, representing loops that trap light forever. Often called photon spheres (Beem *et al.* 1996), these closed curves are tangent to the light cones, which in our case are defined by the two vectors $\eta_\lambda^\pm(x_0)$ (figure 2).

Due to its special non-stretching nature, we refer to a photon sphere of E_1 as a primary photon sphere. Photon spheres of E_λ with $\lambda \neq 1$ will be referred to as secondary photon spheres. A primary photon sphere in our context resists the universally observed material stretching in turbulence: it reassumes its initial arclength at time t. This conservation of arclength, along with the conservation of the enclosed area in the incompressible case, creates extraordinary coherence.

Even if a primary photon sphere does not exist in a region, secondary photon spheres with either $\lambda > 1$ or $\lambda < 1$ may well be present. The largest of these photon spheres marks the end of the family of coherent belts. It will signal either weak stretching ($\lambda > 1$) or weak contraction ($\lambda < 1$) for the vortex it bounds. Weakly compressing Lagrangian vortices are evolving towards even fuller coherence, preserving their enclosed area while smoothing out mild bumps in their boundaries. By contrast, weakly stretching Lagrangian vortices can be viewed as domains of slowly eroding coherence, where a perfect, non-stretching core can no longer be found.

Motivated by these observations, we introduce the following terminology. A *black-hole vortex* is a region surrounded by an outermost (i.e. locally the largest) photon sphere (or *ring*) of the tensor family E_λ. A *primary black-hole vortex* is one that contains at least one primary photon sphere, such as the one shown in figure 2. A *secondary black-hole vortex* is one that only contains secondary photon spheres. Such a vortex is either strengthening ($\lambda < 1$) or weakening ($\lambda > 1$).

5. Detection of Lagrangian vortices

The above analogy with black holes has practical implications for locating Lagrangian vortices in a complex flow. To see this, note that the strain eigenvectors ξ_1 and ξ_2 in (2.7) become ill-defined at points where $\lambda_1(x_0) = \lambda_2(x_0) = 1$. Null-geodesics, such as those forming photon spheres, cannot be extended to such points, because the Green–Lagrange metric g_1 is singular there $[E_1(x_0) = 0]$. These degenerate points are analogues of Penrose–Hawking singularities in cosmology (Hawking & Penrose 1996). Intuitively, one expects that any coherent Lagrangian vortex in the fluid must contain such a singularity in its interior, just as all black holes are expected to contain Penrose–Hawking singularities. This expectation turns out to be correct, leading to the following result (supplementary Appendix D): at time t_0, the interior of a Lagrangian vortex must contain a point x_0^* satisfying $E_1(x_0^*) = 0$. Specifically, only regions containing such points may fully incorporate Lagrangian vortices.

On the basis of these findings, admissible regions for coherent Lagrangian vortices are those with at least one metric singularity $[E_1(x_0^*) = 0]$. In practice, metric singularities tend to cluster, and we only consider clusters surrounded by an annular region with no singularities. In these admissible regions, Lagrangian vortex boundaries are sought as outermost Green–Lagrange photon spheres, i.e. outermost limit cycles of the differential equations (3.2). This process involves conceptually simple numerical steps, but its implementation requires care for noisy observational data (supplementary Appendix F).

6. Lagrangian vortices in the Agulhas leakage

We apply our results to the Agulhas leakage, a by-product of the Agulhas current of the south-west Indian Ocean. At the end of its southward flow, this boundary current turns back on itself, creating a loop that occasionally pinches off and releases eddies (Agulhas rings) into the South Atlantic.

Lagrangian transport by coherent Agulhas rings has implications for global circulation and climate change (Beal *et al.* 2011). As shown by Beron-Vera *et al.* (2013), eddy tracking from instantaneous altimetric sea-surface-height (SSH) measurements (Chelton, Schlax & Samelson 2011) would substantially overestimate the coherent part of this transport. Here, we reconsider the region studied by Beron-Vera *et al.* (2013) and show how the coherent Lagrangian vortex principle developed here uncovers previously unknown material eddies, sharpening available coherent transport estimates. The South Atlantic ocean region in question is bounded by longitudes [14° W, 9° E] and latitudes [39° S, 21° S]. Using satellite altimetry data, we seek coherent Lagrangian vortices (black-hole eddies, for short) over a 90-day time period, ranging from $t_0 =$ 24 November 2006 to $t =$ 22 February 2007. Supplementary Appendix G provides more information on the data and the numerical methods employed.

The computational steps reviewed in supplementary Appendix F yield eight admissible regions for Lagrangian vortices (figure 3*a*). Out of these eight regions, only seven turn out to contain black-hole eddies, bounded by outermost Green–Lagrange photon spheres (figure 3*b*). Two of these are primary black-hole eddies, containing primary photon spheres. The latter curves were previously identified by Beron-Vera *et al.* (2013) as locally most shearing lines from other methods.

Out of the two primary black-hole eddies, eddy 2 has a slightly weakening external boundary with $\lambda = 1.02$, while eddy 3 has a slightly strengthening boundary

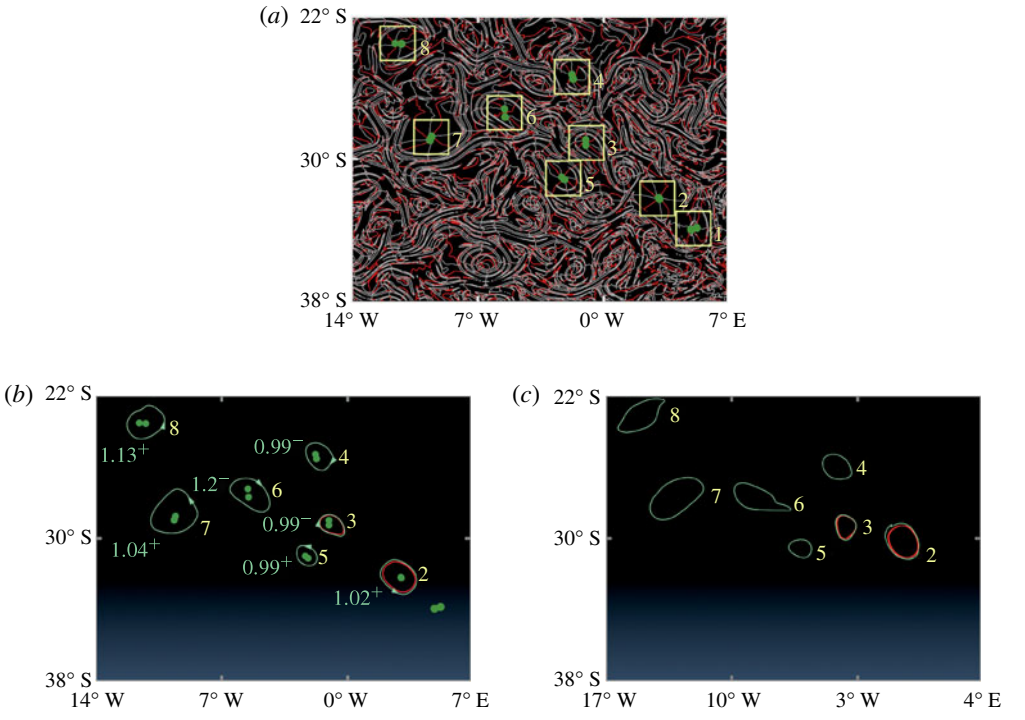

FIGURE 3. (*a*) Green–Lagrange singularities and black-hole eddy candidates on 24 November 2006 (intersections of red and white curves; cf. supplementary Appendix F, step *c*) and admissible Lagrangian vortex regions (yellow). The dark green singularity clusters are surrounded by singularity-free belts of at least 50 km in diameter. (*b*) Black-hole eddy boundaries on 24 November 2006 (light green, with λ values in light green) and primary photon spheres (red). The $\pm$ signs shown are those of $\eta_\lambda^\pm$. (*c*) Advected Lagrangian vortex boundaries 3 months later (on 22 February 2007).

with $\lambda = 0.99$. The boundaries of the secondary black-hole eddies 4 and 5 are also slightly gaining coherence ($\lambda = 0.99$), whereas the secondary eddies 6, 7 and 8 are losing coherence ($\lambda = 1.2$, 1.04 and 1.13, respectively). Accordingly, the boundary of eddy 6 is expected to exhibit the largest degree of stretching. This stretching is still uniform, leaving room for a coherent material belt for the 90-day study period. These conclusions are confirmed by figure 3(*c*), showing the seven advected black-hole eddy boundaries 3 months later.

We verified the theoretically predicted λ stretching values for black-hole eddy boundaries by their direct numerical advection. In this test, we found the λ values obtained from advection to be accurate up to two decimal digits, as listed in the left-bottom panel of figure 3. Since these eddy boundaries are constructed as limit cycles, they are structurally stable, i.e. smoothly persist under small errors and uncertainties in the observational dataset.

The detailed knowledge of black-hole eddies yields specific estimates for their Lagrangian transport rates. As in Goni *et al.* (1997), we assume that the eddies are bounded from below by the isotherm of 10 °C, located roughly at 400 m in the area of study. Under this assumption, we obtain the eddy transport rates shown in table 1. On average, a black-hole eddy moves water north-westward at a rate of about 1.3 Sv

BH eddy									
2	3	4	5	6	7	8	BH average	BH total	SSH total
1.4	1.8	0.8	1.0	1.1	1.0	2.0	1.3	9.1	18

TABLE 1. Transport rates in Sv for black-hole (BH) eddies and SSH eddies on 24 November 2006.

(1 Sv $= 10^6$ m^3 s^{-1}). This represents a 30 % upward refinement to the 1 Sv estimate of Goni *et al.* (1997) for average transport by SSH eddies in the Agulhas leakage. More significant is the difference between the total eddy transport calculated from black-hole eddies and the total eddy transport calculated from SSH eddies using the estimate of Goni *et al.* (1997). As seen from table 1, SSH snapshots significantly overestimate coherent eddy transport.

We note that *in situ* measurements analysed by van Aken *et al.* (2003) reveal some mesoscale eddies reaching depths as large as 2000 m or more, as opposed to the generic 500 m depth assumed by Goni *et al.* (1997) and in the present work. The difference in the previous Eulerian and the present Lagrangian transport estimates increases linearly with the assumed depth for the eddy.

Finally, figure 4(*a*) shows a longer computation of the paths of the seven black-hole eddies. Most preserve their coherence way beyond their 3-month extraction period. Also shown is the evolution of fluid starting from a nonlinear SSH eddy obtained from the analysis of Chelton *et al.* (2011) (figure 4*b*). This illustrates the rapid loss of coherence that fluid initialized in an Eulerian vortex will generically experience in turbulence.

Common Lagrangian diagnostics of material coherence do not fare well either. For instance, the finite-time Lyapunov exponent (FTLE) field displays ridges spiralling into black-hole eddies in the ocean region studied here. This incorrectly signals a lack of coherent material boundaries for Agulhas rings, as noted by Beron-Vera, Olascoaga & Goni (2008).

7. Conclusions

We have given a variational description of coherent Lagrangian vortex boundaries as closed belts of fluid showing no leading-order variability in their averaged material straining. Such material belts are filled with closed null-geodesics of a generalized Green–Lagrange strain metric, which can be computed as limit cycles of a Lagrangian vector field. Outermost members of such limit-cycle families mark observed boundaries of material coherence. Using this approach, we have found exceptionally coherent material belts in the South Atlantic, filled with analogues of photon spheres around black holes. Our results apply to any two-dimensional velocity field, providing a frame-independent way of detecting coherent Lagrangian vortices.

In addition to the transport of diffusive water attributes, the transport of other materials (e.g. garbage or oil contamination) is also expedited by the coherent Lagrangian vortices identified here. Related results on elliptic regions in steady inertial particle motion (Haller & Sapsis 2008) suggest that these vortices will capture and swallow nearby passively floating debris. Thus, beyond the mathematical equivalence, there are also observational reasons for viewing coherent Lagrangian eddies as black holes.

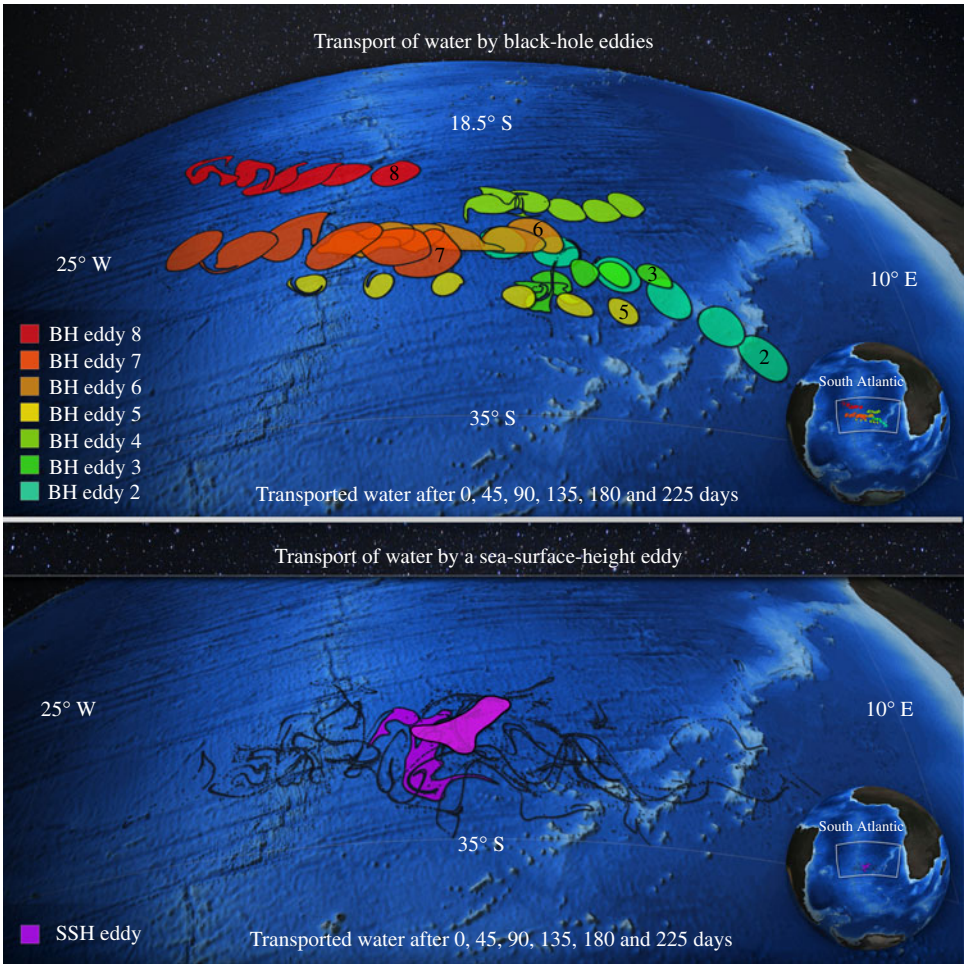

FIGURE 4. (*a*) The evolution of black-hole eddies (extracted from 3 months of data) in the South Atlantic over a period of 225 days. The eddies move from east to north-west (from right to left). (*b*) The material evolution of a nonlinear SSH eddy over the same 225 days.

Continually available observational data for the ocean are limited to two spatial dimensions. However, the existence of a coherent material belt outside down- or upwellings should already be well-captured by two-dimensional altimetry data. We therefore also expect black-hole-type vortices to be present in two-dimensional atmospheric wind data, framing the Lagrangian footprints of hurricanes on Earth and of the Great Red Spot on Jupiter.

Acknowledgements

The altimetry data used here are available from AVISO (http://aviso.oceanobs.com). G.H. acknowledges partial support by NSERC grant 401839-11. FJBV acknowledges support by NSF grant CMG0825547, NASA grant NNX10AE99G and by a grant from the British Petroleum/The Gulf of Mexico Research Initiative.

Supplementary material

Supplementary material are available at http://dx.doi.org/10.1017/jfm.2013.391.

References

ARNOLD, V. I. 1973 *Ordinary Differential Equations*. Massachusetts Institute of Technology.

BEAL, L. M., DE RUIJTER, W. P. M., BIASTOCH, A., ZAHN, R. & SCOR/WCRP/IAPSO WORKING GROUP, 2011 On the role of the Agulhas system in ocean circulation and climate. *Nature* **472**, 429–436.

BEEM, J. K., EHRLICH, P. L. & KEVIN, L. E. 1996 *Global Lorentzian Geometry*. CRC Press.

BERON-VERA, F. J., OLASCOAGA, M. J. & GONI, G. J. 2008 Oceanic mesoscale vortices as revealed by Lagrangian coherent structures. *Geophys. Res. Lett.* **35**, L12603.

BERON-VERA, F. J., WANG, Y., OLASCOAGA, M. J., GONI, G. J. & HALLER, G. 2013 Objective detection of oceanic eddies and the Agulhas leakage. *J. Phys. Oceanogr.* **43**, 1426–1438.

CHELTON, D. B., SCHLAX, M. G. & SAMELSON, R. M. 2011 Global observations of nonlinear mesoscale eddies. *Prog. Oceanogr.* **91**, 167–216.

DENMAN, K. L. & GARGETT, A. E. 1983 Time and space scales of vertical mixing and advection of phytoplankton in the upper ocean. *Limnol. Oceanogr.* **28**, 801–815.

FROYLAND, G., HORENKAMP, C., ROSSI, V., SANTITISSADEEKORN, N. & GUPTA, A. S. 2012 Three-dimensional characterization and tracking of an Agulhas ring. *Ocean Model.* **52–53**, 69–75.

GONI, G. J., GARZOLI, S. L., ROUBICEK, A. J., OLSON, D. B. & BROWN, O. B. 1997 Agulhas ring dynamics from TOPEX/Poseidon satellite altimeter data. *J. Mar. Res.* **55**, 861–883.

HALLER, G. 2005 An objective definition of a vortex. *J. Fluid Mech.* **525**, 1–26.

HALLER, G. & SAPSIS, T. 2008 Where do inertial particles go in fluid flows? *Physica* D **237**, 573–583.

HAWKING, S. & PENROSE, R. 1996 *The Nature of Space and Time*. Princeton University Press.

JEONG, J. & HUSSAIN, F. 1985 On the identification of a vortex. *J. Fluid Mech.* **285**, 69–94.

PROVENZALE, A. 1999 Transport by coherent barotropic vortices. *Annu. Rev. Fluid Mech.* **31**, 55–93.

TRUESDELL, C. & NOLL, W. 2004 *The Nonlinear Field Theories of Mechanics*. Springer.

VAN AKEN, H. M., VAN VELDHOVENA, A. K., VETHA, C., DE RUIJTERB, W. P. M., VAN LEEUWENB, P. J., DRIJFHOUTC, S. S., WHITTLED, C. P. & ROUAULTD, M. 2003 Observations of a young Agulhas ring, *Astrid, during MARE in March 2000. Deep-Sea Res.* II **50**, 167–195.